NeuroImage: Clinical 36 (2022) 103274

Contents lists available at ScienceDirect

NeuroImage: Clinical

journal homepage: www.elsevier.com/locate/ynicl

3T sodium MR imaging in Alzheimer's disease shows stage-dependent sodium increase influenced by age and local brain volume

Alexa Haeger [a,b], Fawzi Boumezbeur [c], Michel Bottlaender [c,d], Cécile Rabrait-Lerman [c], Julien Lagarde [d,e,f], Shahram Mirzazade [a,b], Janna Krahe [a,b], Christian Hohenfeld [a,b], Marie Sarazin [d,e,f], Jörg B. Schulz [a,b], Sandro Romanzetti [a,b,1], Kathrin Reetz [a,b,*,1]

[a] Department of Neurology, RWTH Aachen University, Aachen, Germany
[b] JARA-BRAIN Institute Molecular Neuroscience and Neuroimaging, Forschungszentrum Jülich GmbH and RWTH Aachen University, Aachen, Germany
[c] NeuroSpin, CEA, CNRS UMR9027, Paris-Saclay University, Gif-sur-Yvette, France
[d] Paris-Saclay University, CEA, CNRS, Inserm, BioMaps, Service Hospitalier Frédéric Joliot, Orsay, France
[e] Department of Neurology of Memory and Language, GHU Paris Psychiatrie & Neurosciences, Hôpital Sainte Anne, F-75014 Paris, France
[f] Université Paris-Cité, F-75006 Paris, France

ARTICLE INFO

Keywords:
Sodium-23 (^{23}Na)
Sodium MRI
Alzheimer's Disease (AD)
Magnetic resonance imaging (MRI)
Aging
Metabolism

ABSTRACT

Introduction: Application of MRI in clinical routine mainly addresses structural alterations. However, pathological changes at a cellular level are expected to precede the occurrence of brain atrophy clusters and of clinical symptoms. In this context, ^{23}Na-MRI examines sodium changes in the brain as a potential metabolic parameter. Recently, we have shown that ^{23}Na-MRI at ultra-high-field (7 T) was able to detect increased tissue sodium concentration (TSC) in Alzheimer's disease (AD). In this work, we aimed at assessing AD-pathology with ^{23}Na-MRI in a larger cohort and on a clinical 3T MR scanner.

Methods: We used a multimodal MRI protocol on 52 prodromal to mild AD patients and 34 cognitively healthy control subjects on a clinical 3T MR scanner. We examined the TSC, brain volume, and cortical thickness in association with clinical parameters. We further compared TSC with intra-individual normalized TSC for the reduction of inter-individual TSC variability resulting from physiological as well as experimental conditions. Normalized TSC maps were created by normalizing each voxel to the mean TSC inside the brain stem.

Results: We found increased normalized TSC in the AD cohort compared to elderly control subjects both on global as well as on a region-of-interest-based level. We further confirmed a significant association of local brain volume as well as age with TSC. TSC increase in the left temporal lobe was further associated with the cognitive state, evaluated *via* the Montreal cognitive assessment (MoCA) screening test. An increase of normalized TSC depending on disease stage reflected by the Clinical Dementia Rating (CDR) was found in our AD patients in temporal lobe regions. In comparison to classical brain volume and cortical thickness assessments, normalized TSC had a higher discriminative power between controls and prodromal AD patients in several regions of the temporal lobe.

Discussion: We confirm the feasibility of ^{23}Na-MRI at 3T and report an increase of TSC in AD in several regions of the brain, particularly in brain regions of the temporal lobe. Furthermore, to reduce inter-subject variability caused by physiological factors such as circadian rhythms and experimental conditions, we introduced normalized TSC maps. This showed a higher discriminative potential between different clinical groups in comparison to the classical TSC analysis. In conclusion, ^{23}Na-MRI represents a potential translational imaging marker applicable e.g. for diagnostics and the assessment of intervention outcomes in AD even under clinically

Abbreviations: AD, Alzheimer's Disease; ATP, Adenosine-triphosphate; AUC, Area under the curve; BDI, Beck Depression Inventory; CDR, Clinical Dementia Rating; CERAD, Consortium to Establish a Registry for Alzheimer's Disease; CT, Cortical Thickness; CVF, Cell Volume Fraction; CSF, Cerebrospinal fluid; FPR, False Positive Rate; FA, Flip Angle; FOV, Field-of-view; GM, Grey Matter; MoCA, Montreal Cognitive Assessment; MMSE, Mini Mental State Examination; MRI, Magnetic Resonance Imaging; PET, Positron Emission Tomography; ROC, Receiver Operating Characteristics; ROI, Region of Interest; SD, Standard deviation; SNR, Signal-to-Noise-Ratio; TBM, Tensor-based-morphometry; TPR, True Positive Rate; TSC, Tissue sodium concentration; WM, White Matter.

* Corresponding author at: Department of Neurology, University Hospital, RWTH Aachen University, Pauwelsstraße 30, 52074 Aachen, Germany.
E-mail address: kreetz@ukaachen.de (K. Reetz).

[1] Contributed equally.

https://doi.org/10.1016/j.nicl.2022.103274
Received 1 March 2022; Received in revised form 12 November 2022; Accepted 20 November 2022
Available online 21 November 2022

available field strengths such as 3T. Implication of ^{23}Na-MRI in association with other metabolic imaging marker needs to be further elucidated.

1. Introduction

Alzheimer's disease (AD) is the most common form of dementia. According to current demographic developments, AD is expected to affect a rising number of people in the future, together with a significantly increased affected lifetime of the patients, representing a major public health challenge (Holtzman et al., 2011; Nichols et al., 2019). The absence of effective disease-modifying treatments underlines the need to advance the development of novel therapeutic strategies for addressing this urgent and immediate medical challenge (Scheltens et al., 2021). Crucially, the development of novel treatments is limited by an insufficient understanding of the pathological processes underlying the development and progression of dementia (Huang et al., 2020) and focus especially needs to be set on the earliest stages of neurodegeneration (Cummings et al., 2007; Scheltens et al., 2021). Currently, cerebrospinal fluid (CSF) and Positron-Emission-Tomography (PET) are used in clinical practice to detect pathological hallmarks such as amyloid plaques and tau tangles (Jack et al., 2018; Nordberg et al., 2010). Since these techniques do not always reflect the degree of clinical impairment, non-invasive methods such as MR imaging (MRI) are already integrated in clinical scanning routines, possibly leading to an improved understanding of metabolic changes in prodromal AD. So far, MRI has mainly focused on the detection of volumetric alterations in the pathway for clinical diagnosis of AD (Fox et al., 2000; Frisoni et al., 2010; McDonald et al., 2009). However, complementary MRI techniques are available, in particular sodium MRI (^{23}Na-MRI). This technique has been shown to be sensitive to increases in local tissue sodium levels reflecting jeopardized cell viability and preceding cell death (Boada et al., 2005). Therefore, sodium imaging has been used in the context of cerebral infarction, tumor lesions, inflammatory diseases such as multiple sclerosis, and in neurodegeneration (Inglese et al., 2010; Nielles-Vallespin et al., 2007; Reetz et al., 2012; Regnery et al., 2020; Shah et al., 2016; Thulborn, 2018; Thulborn et al., 1999). Sodium increase has been shown to be a relevant aspect in AD, since *post mortem* studies have indicated ion disbalances such as sodium increases in AD (Graham et al., 2015; Vitvitsky et al., 2012), possibly as a consequence or accompanying phenomenon of energy deficits and change of ion channel expression in AD. However, ^{23}Na-MRI is a challenging technique that requires state-of-the-art acquisition strategies and possibly high or ultra-high magnetic field strengths to overcome the intrinsic low MR sensitivity of the sodium nucleus (Haeger et al., 2021; Romanzetti et al., 2014).

Recently, we used ^{23}Na-MRI in AD patients on a ultra-high-field (7 T) MR scanner, and were able to show sodium increases in several brain regions, associated with tau-pathology assessed by Flortaucipir-PET imaging in AD (Haeger et al., 2021). ^{23}Na-MRI could therefore be a valuable tool for detecting metabolic energy depletion in AD interacting with AD-pathology and help shifting the focus on metabolic disbalances on cellular level as possible earliest starting point of the disease, with a further dynamic development of energy disbalances during disease progression.

The aim of this study was to combine high-resolution volumetric assessments routinely performed on a 3T high-field MR scanner with ^{23}Na-MRI as a possible metabolic imaging technique and to put these in relation to standard clinical assessments. The resulting outcome would shed light about the potential of ^{23}Na-MRI as an imaging biomarker for neurodegeneration on a clinical 3T MR scanner, possibly preceding or accompanying brain atrophy and aging. We therefore performed ^{23}Na-MRI on a large sample of altogether 86 subjects comprising AD patients at different stages of the disease as well as healthy control subjects from younger to advanced age to examine influences of atrophy, age and gender on cerebral sodium content at 3T field conditions.

2. Materials and methods

2.1. Study participants

A total of 86 subjects, comprising 52 patients with AD (20 female, mean age 70.4 ± 6.1 years), 20 age-matched elderly control subjects (4 female, mean age 67.8 ± 9.4 years) as well as 14 younger control subjects for analysis of age-related effects (5 female, mean age 29.2 ± 6.4 years) participated in the study.

All twenty elderly control subjects met the following criteria: (1) Mini-Mental State Examination (MMSE) score ≥ 27 and (2) normal neuropsychological assessments and/or no further report of subjective memory impairment, (3) no history of chronic psychiatric or central neurological conditions. Study participants received cognitive assessment, including cognitive screening tests with the Mini Mental State Examination (MMSE) (Folstein et al., 1975) for all control subjects, and further the Consortium to Establish a Registry for Alzheimer's Disease (CERAD Plus) (47). The (1) Clinical Dementia Rating (CDR) (Morris, 1993) as well as the (2) MoCA scores were used as an indicator for the severity of the dementia grade of all participants according to the NICE-guidelines (https://www.nice.org.uk/guidance/ng97). Diagnosis of AD was confirmed in accordance with the international criteria of the National Institute on Aging and Alzheimer's association NIA-AA-research framework. Part of the AD cohort came from the Dementia-MOVE-study (Haeger et al., 2020). To fulfill AD biomarker research criteria, 51 out of 52 AD patients had undergone lumbar puncture with evaluation of neurodegenerative markers beforehand (pathological range: amyloid β1-42 < 450 pg/ml, amyloid β1-42/40 ratio < 0.5, total tau > 450 pg/ml and phosphorylated tau > 61 pg/ml), analysis being performed in the Neurochemical Laboratory at the University of Göttingen (Reiber, 2005; Zettl et al., 2005).

AD patients were separated in a less affected group (CDR = 0 or 0.5) and a more dependent group (CDR = 1 or 2). Control subjects younger than 40 years old did not receive the complete cognitive battery. To detect behavioral disturbances and depression, the Beck Depression Inventory-II (BDI) (Beck et al., 1996) was further applied. The elderly control group was age-matched to the patient's group. The study was approved by the local ethics committee of the RWTH Aachen University (EK 083/15 and EK 306/18 [Dementia-Move]) and was conducted according to the guidelines of the declaration of Helsinki. An overview of the study sample is given in Table 1. All subjects gave their written informed consent before participating.

2.2. MR protocol and image processing

All MRI scans were performed on a 3T whole body scanner (PRISMA 3T, Siemens Healthineers, Erlangen, Germany). The scanning session comprised ^{23}Na- and ^{1}H-imaging. ^{23}Na-MRI scans were performed using a double resonant ^{1}H/^{23}Na quadrature birdcage coil (Rapid Biomed GmbH, Rimpar, Germany). A Variable-Flip-Angle method (VFA) was used to obtain quantitative TSC maps (Coste et al., 2019). Briefly, two successive scans with a gradient-spoiled 3D FLORET sequence (Madelin and Regatte, 2013; Pipe et al., 2011) (TR = 20 ms, TE = 0.1 ms, FOV = 256 mm, 4 mm isotropic resolution, 3 acquisition blocks of 3 min per scan) were acquired at a different flip angle (FA1/FA2 = 25°/55°). In addition, the B_1^+ field was estimated using the Double Angle Method (FA1/FA2 = 60°/120°, TR/TE = 80 ms/0.1 ms, 6 mm isotropic resolution) to correct for residual B1-inhomogeneities. The two sodium images and the B_1^+ field were combined as described elsewhere (Coste

Table 1
Illustration of the demographic data of our sample with effect-sizes of comparison between Alzheimer patients and elderly control subjects. Mean values ± Standard deviation are illustrated, with minima and maxima in brackets. Y = years, MoCA = Montreal cognitive assessment, MMSE = Mini Mental state examination, CDR = clinical dementia rating, BDI = Beck Depression Inventory. [1] for controls $n = 16/20$; [2] for patients $n = 51/52$; [3] $n = 18/20$; [4] for patients: $n = 36/52$, for controls: $n = 16/20$; [5] for patients: $n = 44/52$ for controls: $n = 13/20$; [6] for patients $n = 41/52$, for controls: $n = 16/20$; [7] for patients $n = 42/52$, for controls: $n = 16/20$; [8] for patients $n = 51/52$; [9] for patients $n = 50/52$.

		AD patients	Elderly Control subjects	
	Mean ± SD [min,max]	$n = 52$	$n = 20$	*p*-value
Demographics	Age, y	70.4 ± 6.1 [53, 80]	68.0 ± 9.3 [49, 81]	0.2
	Gender F/M	20/32	4/16	–
	Education, y	13.3 ± 3.5 [5, 22]	15.3 ± 3.5 [10, 20][1]	0.05
	Disease Duration, y	2.8 ± 1.7 [0, 7]	–	–
Neuropsychology	MoCA (/30)	19.8 ± 5.1 [9, 28] [2]	27.9 ± 1.3 [26, 30]	**<0.001**
	MMSE (/30)	24.8 ± 3.6 [16, 30]	29.3 ± 1.0 [27, 30] [3]	**<0.001**
	CDR = 0/0.5/1/2	8/25/18/1	20/0/0/0	–
	BDI[4]	8.1 ± 6.4 [0, 25]	2.8 ± 2.7 [0, 10]	**0.002**
	Word List Fixation[5]	13.8 ± 5.7 [4, 30]	21.6 ± 4.1 [14, 29]	**<0.001**
	Word List Recall[5]	3.0 ± 2.5 [0, 10]	7.5 ± 1.9 [4, 10]	**<0.001**
	Word List Recogn. [5]	16.8 ± 2.3 [12, 20]	19.5 ± 0.7 [18, 20]	**<0.001**
	Visuoconstr. [5]	9.1 ± 3.0 [0, 11]	10.8 ± 0.6 [9, 11]	0.05
	Visuoconstr. Recall[5]	4.9 ± 3.7 [0, 11]	9.7 ± 1.4 [7, 11]	**<0.001**
	Phonematic Fluency[6]	11.4 ± 4.4 [2, 22]	16.8 ± 5.4 [8, 27]	**<0.001**
	Semantic Fluency[5]	13.5 ± 5.7 [3, 28]	22.8 ± 5.0 [16, 33]	**<0.001**
	Boston Naming[5]	13.3 ± 2.6 [3, 15]	14.8 ± 0.4 [14, 15]	**0.03**
	Trail Making A in s[6]	65.1 ± 46.4 [26, 268]	36.7 ± 14.3 [20, 67]	**0.02**
	Trail Making B in s[7]	200.5 ± 86.9 [69, 300]	104.1 ± 58.5 [38, 300]	**< 0.001**
CSF markers	CSF β-amyloid 1–42[8]	418.4 ± 143.7 [135, 812]	–	–
	CSF β -amyloid 1–40[9]	11711.5 ± 4646.4 [711, 25356]	–	–
	β -amyloid Ratio[9]	0.36 ± 0.10 [0.06, 0.53]	–	–
	CSF p-tau[8]	93.4 ± 32.1 [36, 191]	–	–
	CSF tau[8]	727.1 ± 626.2 [201, 4664]	–	–

et al., 2019). The resulting sodium image was then corrected for partial volume effects using an iterative Van-Cittert approach (Thomas et al., 2016). Finally, TSC maps were obtained by applying a linear two-point calibration utilizing the signal of two calibration tubes of known sodium concentrations of 51 mmol/l and 102 mmol/l placed next to the subjects' heads. TSC maps were then co-registered to the T_1-weighted anatomical reference in inverse contrast from the ^{1}H protocol, comprising a high-resolution anatomical T_1-weighted brain scans using an MPRAGE sequence (TR = 2300 ms, TI = 900 ms, TE = 2.3 ms, FA = 7°, TA = 7 min, 0.8 mm isotropic resolution). An overview of the ^{23}Na-MR-analysis is given in Fig. 1. Details of our image-processing pipeline are presented in the Supplementary Materials of this manuscript.

The Hammersmith Segmentation Atlas (Hammers et al., 2003) as well as the VolBrain Segmentation atlas (Manjón and Coupé, 2016) were used for our region-of-interest (ROI) based analysis. CSF was removed from all masks to isolate brain tissue and exclude possible "spill-in" effects from high CSF sodium concentrations and results on the 32 brain regions reported. To maintain the original anatomical shape of the mask, no erosion was performed. For regional volume calculation, each ROI volume was corrected for total intracranial volume. We further determined the regional cortical thickness in ANTs (Tustison et al., 2014).

For each ROI, the sodium content was calculated as the median of the regional TSC distribution extracted from each quantitative TSC map. The median was considered to account for the non-gaussian distribution of the TSC signal in the ROIs.

2.3. Normalization of TSC

To take into account a possible inter-individual variability of TSC maps caused by physiological effects such as circadian rhythms (Harrington et al., 2010), and slightly different experimental conditions utilized in the sodium acquisition sessions, we employed a normalization method used in PET-imaging (de Souza et al., 2011; Goutal et al., 2020). This consisted in a global normalization of TSC maps to the mean TSC inside the brain stem mask of the Hammersmith atlas in FSL (Jenkinson et al., 2012). The brain stem mask was eroded by 4 mm to exclude any CSF influence. The brain stem was selected similar to PET-imaging, because it is expected to be the most stable region with respect to metabolic hypometabolism in AD (Ishii, 2002; Bauer, 2013). These observations were also confirmed from our own 7 T ^{23}Na-MRI study at 3 mm isotropic resolution (Haeger et al., 2021). All following analyses were performed with both approaches in this paper: classical quantitative TSC in mmol/l for quantification and normalized TSC for comparison purposes.

2.4. Statistical analysis

2.4.1. Voxel-based whole brain analyses

Voxel-based whole brain analyses on (A) T_1-weighted anatomical images and (B) quantitative TSC and (C) normalized TSC were performed to detect group differences on a structural and metabolic level, respectively. The study group was used to create an anatomical template as well as a sodium template in ANTs (Avants et al., 2011).

For (A), structural analysis was done by means of a tensor-based-morphometry (TBM) analysis. Log Jacobians of the geometrical transformations of individual T1-weighted images to a minimal deformation group template from the control cohort were compared voxel-wise by a permutation analysis ($n = 2000$) performed with BROCCOLI (Eklund et al., 2014) only on voxels inside the brain tissue mask, including CDR (0; 0.5; 1 or 2, and setting age and gender as covariates). For (B) and (C), a likewise permutation analysis ($n = 2000$ permutations) was performed again on voxels within the brain tissue mask after smoothing ($\sigma = 2$ mm), including again CDR (0; 0.5; 1 or 2) and age and gender as covariates. The resulting *t*-values of the cluster-based statistics were reported at a corrected $p < 0.05$ level of significance.

2.4.2. ROI-based analysis

ROI-based group analysis was performed to inspect our multimodal imaging datasets on regional level. Regional quantitative TSC for quantification, normalized TSC, cortical thickness and volume (the volume normalized for total intracranial volume) were compared between patients and controls via Wilcoxon Rank Sum test and Bonferroni-Holm-corrected for multiple comparisons in MATLAB (Version R2019b, Mathworks) for each modality analyzed. ROIs from left and right hemispheres were averaged calculating the mean between individual left and right ROIs.

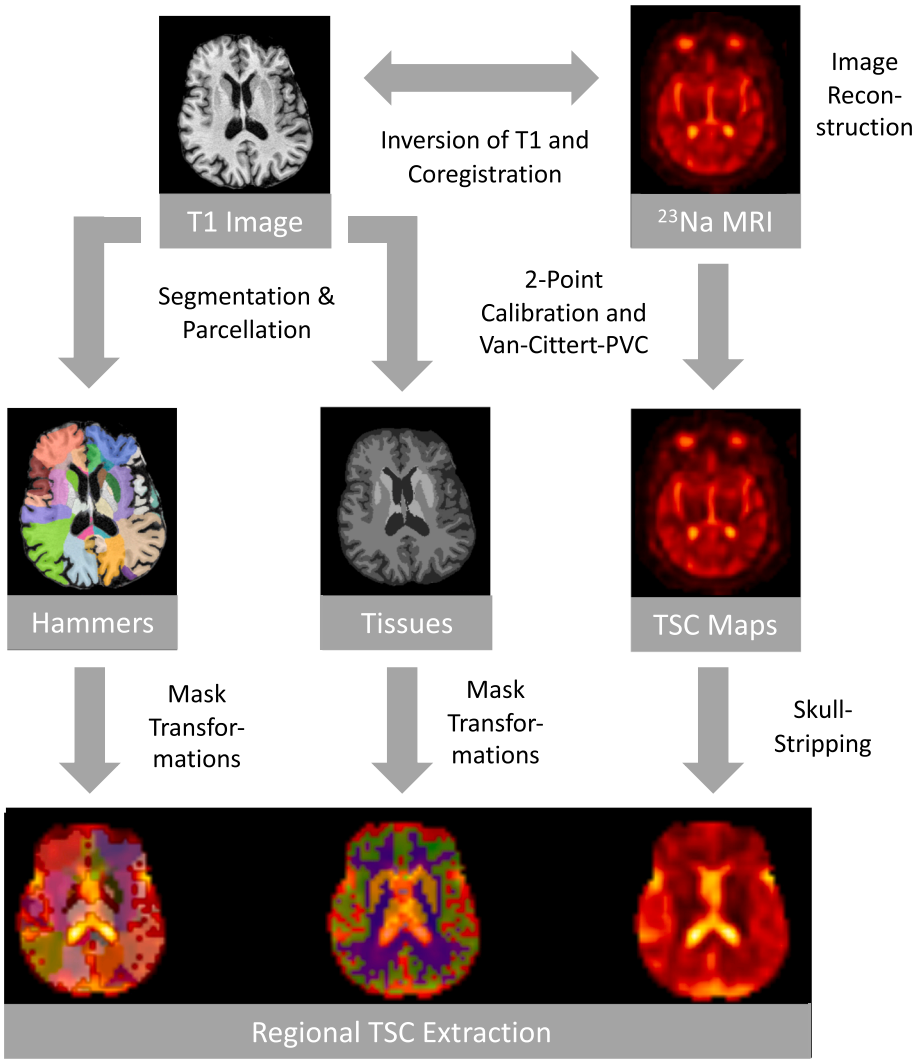

Fig. 1. Illustration of the processing steps of ^{23}Na-MRI: Following reconstruction, denoising and correction for B_1-inhomogeneity, total sodium concentration maps are obtained after Van-Cittert-partial volume correction (Thomas et al., 2016) from the ^{23}Na M_0-images via a 2-point calibration. TSC maps are then co-registered to their corresponding T_1-weigthed inverted anatomical reference (B). CSF, WM, GM segmentation masks as well as Hammersmith and VolBrain atlas parcellation from T_1-weighted anatomical reference are calculated and transformed into the original ^{23}Na-MRI space. Regional TSC values as well as normalized TSC are extracted from partial volume corrected TSC images.

2.4.3. Multiple regression analysis: Influence of regional volume on regional TSC

To further regress out the influence of regional volume, as well as age and gender on regional TSC, multiple regression models of TSC ~ Volume + Age + Gender were calculated for the patient's as well as the elderly control group for a preselection of regions representative for each lobe in MATLAB (Version R2019b, Mathworks) and Residuals of TSC statistically compared via Wilcoxon Rank Sum test again in a second step, to examine group differences independent of regional volume, age and gender effects. This was performed on quantitative maps of TSC as well as on normalized TSC.

2.4.4. Voxel-based regression analysis for the association between TSC and cognition

To further analyze which brain regions with TSC increase are associated with cognitive decline, a voxel-wise regression analysis including multimodal imaging with both ^{23}Na-imaging and structural imaging was included. This was calculated with VoxelStats (Mathotaarachchi et al., 2016) in MATLAB, using a multiple regression model defining MoCA ~ Sodium + Anatomical + Age + Gender. Anatomy, age and gender were included in this model in order to take age, gender and structural effects into consideration. Only patients were included in this analysis. Cognition was here represented by the short cognitive screening test of MoCA. Individual sodium images were transformed into template space, the template coming from *miccai2012-multi-atlas-challenge-data*, its original MRI scans coming from *OASIS* (https://www.oasis-brains.org/). T1-images were also transformed into template space and modulated using the Jacobian determinants. Images were smoothed ($\sigma = 2$ mm) and rescaled. A random field theory (RFT)-correction at $p < 0.05$ was performed at a FWHM of 6 in a second step. This analysis was both done on the quantitative TSC maps as well as the normalized TSC and results from both analyses reported.

2.4.5. ROC-analysis of normalized TSC compared to quantitative TSC, cortical thickness and local brain volume

We repeated our ROI analysis of stage-dependent comparison of TSC between groups with a focus on temporal brain regions by extracting the median of the quantitative TSC maps and normalized TSC from voxels inside ROIs. We then evaluated the effectiveness of regional normalized TSC in distinguishing between elderly controls and mildly affected AD patients with a CDR of 0 or 0.5 ($n = 33$) by receiver operating characteristics (ROC)-analysis, illustrating true positive rate (TPR) against the false positive rate (FPR) and reporting the area under the curve (AUC) in MATLAB. For comparison of predictive potential of normalized TSC versus regional brain volume, we also used the quantitative TSC, normalized regional brain volume and cortical thickness (CT) to compare AUCs between the different parameters.

3. Results

3.1. Voxel-wise based analysis

Whole brain analyses of quantitative TSC maps showed increased TSC in hippocampal regions, however, clusters did not survive significance thresholding at $p < 0.05$ after permutation (see also Fig. 2B). This was also the case when analyzing the subgroups of AD with CDR = 0/0.5 and CDR = 1/2 compared to the elderly controls on whole brain level. On the other hand, for normalized TSC, we found widespread TSC increases with a focus on temporal and occipital regions. There was no difference on whole brain level between patients with CDR 0/0.5 and 1/2. For atrophy clusters, significant clusters were detected for bilateral hippocampus, parahippocampus as well as the right lateral occipital lobe. Patients with CDR 0 and 0.5 revealed atrophy clusters in right hippocampus and parahippocampus as well as right temporal lobe structures, whereas patients with CDR = 1/2 showed atrophy clusters in bilateral hippocampus, parahippocampus, right lateral occipital lobe, bilateral insula, posterior and anterior cingulum.

3.2. ROI-based analysis

We then examined group differences at the regional level. TSC in grey matter (GM) in AD patients was estimated at 47.9 mmol/l ± 6.2 (median ± SD) versus 47.5 mmol/l ± 4.5 in elderly controls (zval = 0.37; p = 0.71) while TSC in white matter (WM) was 38.7 mmol/l ± 5.3 in patients and 39.6 mmol/l ± 3.8 in controls (zval = 0.92; p = 0.36). Sodium content in ventricles in AD patients was 107.2 mmol/l ± 11.0 compared to 102.9 mmol/l ± 11.4 (zval = 1.49; p = 0.14) in elderly controls. Younger control subjects had a median TSC in WM and GM of 34.5 mmol/l ± 5.0 and 39.6 mmol/l ± 4.4, respectively, and 85.7 mmol/l ± 10.3 in CSF. An overview of the TSC values for different ROIs is given in Table 2. Overall, AD patients showed increase in TSC in most ROIs compared to elderly controls, whereas this was not the case for regions of the basal ganglia. ROIs with increased TSC mainly concerned temporal brain regions such as the hippocampus. When correcting for multiple comparisons, there were no significant group differences remaining for the quantitative TSC. For normalized TSC, most ROIs showed highly significant group differences, as already confirmed from our group analyses (see Fig. 3 below). An overview of the normalized TSC, volumetric and CT results is given in Table S1 in the supplementary part of this manuscript.

3.3. Stage-dependent regional TSC, CT and volume alterations

We split our cohort of AD patients in a clinically less (CDR = 0 or 0.5, $n = 33$) and a more affected group (CDR = 1 or 2, $n = 19$) and compared TSC, CT and volume in a preselection of brain regions representative for different brain lobes and consistently affected by neurodegeneration. We found evidence for stage-dependent TSC increases in the AD cohort especially for temporal regions such as the hippocampus. In addition to the temporal lobe, several brain regions from other lobes do show a stage-dependent effect, such as the frontal lobe, basal ganglia and cerebellum as well as the brain stem. For an overview, see also Figure S1 in the supplementary material.

When comparing TSC values in the elderly population compared to the younger controls, there are significant differences in TSC, confirming the influence of age and volume on TSC (Thulborn et al., 2016). Correspondingly, when considering volume and CT alterations in our cohort, we see significant stepwise decreases in our elderly cohort compared to our younger subjects.

3.4. Age- and volume influence on TSC

We further analyzed the influence of local brain volume, age and gender on TSC in 3T MRI. Most ROIs revealed a significant influence especially of age, but also of brain volume on local TSC. ANOVA showed a significant influence of age on all brain regions except for the thalamus. Several regions also pointed to a significant influence of local brain volume: hippocampus, anterior middle temporal lobe, superior temporal gyrus, posterior temporal lobe, anterior and posterior cingulum, superior parietal lobe and corpus callosum, the last showing the strongest effect together with the hippocampus and the posterior temporal lobe. Several regions also revealed an effect of gender on local TSC (Thulborn, 2022), such as regions of the temporal lobe, but also the middle frontal gyrus, the inferior parietal lobe and the lateral occipital gyrus and the corpus callosum (Detailed results presented in Fig. 4 as well as in Table S2 from the supplementary material). The same influence of gender was not observed for normalized TSC maps (Fig. S2).

In a second step, we compared residuals after regressing out the

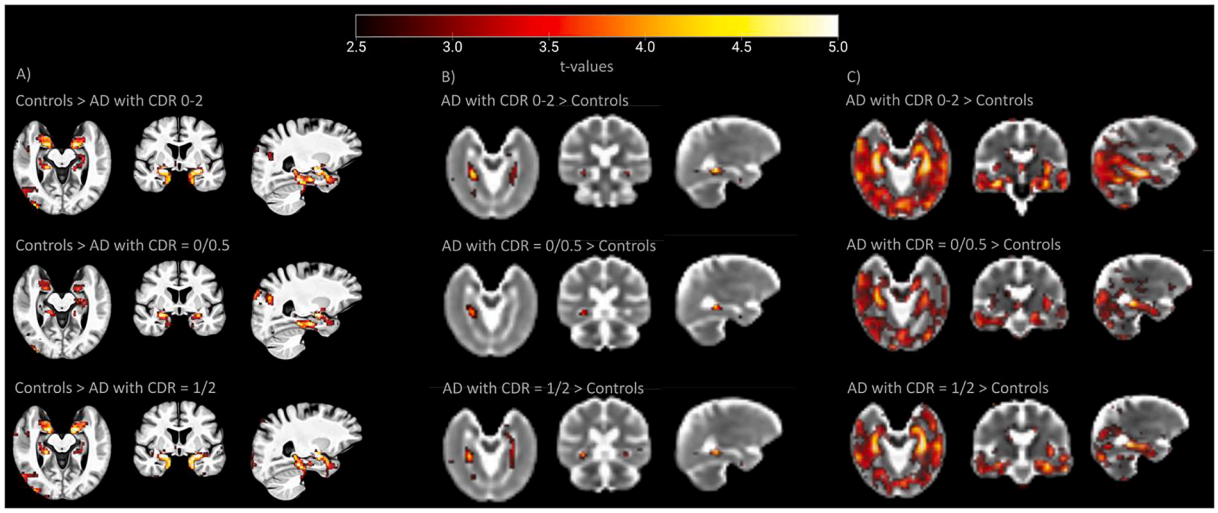

Fig. 2. Illustration of the results from the voxel-wise analysis on whole brain level with presentation of A) TBM results, revealing significant atrophy clusters with a main focus on temporal lobe/hippocampal regions and parietal regions. B) Illustration of voxel-wise permutation analysis on the quantification maps of TSC, with bihippocampal cluster not surviving correction at $p < 0.05$; *t*-values here are presented uncorrected at $p < 0.05$, $n = 2000$ permutations; C) Illustration of the results from normalized TSC-maps, revealed widespread significant clusters with increased normalized TSCs in AD compared to all controls; In sub-analyses, AD with a CDR of 0 or 0.5 show increased clusters with a main focus on temporal, occipital and parietal lobes; AD with a CDR of 1 or 2 reveal similar clusters with also spread into frontal regions. No significant clusters are present for the contrast CDR 0/0.5 versus CDR 1/2, showing no stage-dependent effect on whole brain voxel-level.

Table 2
Median of TSC and standard deviation for left/right averaged ROIs of the Hammersmith atlas for younger controls (n = 14), elderly controls (n = 20), and AD patients (n = 52).

ROI (left/right averaged) from Hammersmith or VolBrain (if noted*) atlas	TSC median Young Controls	TSC STD Young Controls	TSC median Elderly Controls	TSC STD Elderly Controls	TSC median Patients	TSC STD Patients
hippocampus*	42.22	4.45	49.10	5.34	54.23	8.74
amygdala	40.79	4.69	43.77	3.91	46.89	7.92
anterior medial temporal lobe	41.52	4.13	46.19	3.44	47.61	6.70
anterior lateral temporal lobe	42.10	5.67	48.27	4.14	49.53	6.68
ambient and parahippocampus gyri	40.71	5.62	44.25	3.55	48.17	6.80
superior temporal gyrus	39.80	4.69	46.04	4.66	47.00	6.02
inferior middle temporal gyri	37.02	4.81	41.47	4.05	42.36	6.04
fusiform gyrus	38.34	4.66	41.47	4.03	43.70	6.38
cerebellum	36.21	3.78	39.47	4.34	37.82	6.17
brainstem	33.36	4.95	36.89	4.42	33.99	5.57
insula	35.81	4.77	39.71	3.70	38.26	5.41
lateral occipital lobe	38.50	4.86	42.43	3.52	43.31	6.42
anterior cinguli gyrus	37.95	4.66	44.72	4.88	43.98	6.66
posterior cinguli gyrus	37.04	4.48	44.25	4.66	44.95	6.10
middle frontal gyrus	34.91	4.66	42.14	4.50	40.28	5.51
posterior temporal lobe	38.09	4.74	42.90	3.76	44.22	6.12
inferior lateral pariatal lobe	37.64	4.44	45.39	4.44	45.75	6.45
caudate nucleus*	40.28	5.61	50.60	7.39	48.82	6.66
accumbens nucleus	33.52	5.76	37.41	6.00	37.22	8.11
putamen*	31.81	4.94	34.27	4.12	31.90	5.45
thalamus*	31.37	4.89	34.59	4.56	32.12	5.35
pallidum*	29.00	5.56	32.15	4.04	30.11	5.64
corpus callosum	35.30	6.09	43.37	6.64	43.21	8.43
precentral gyrus	32.57	4.73	40.20	4.13	37.72	5.74
gyrus rectus	44.07	5.08	50.03	4.56	49.58	7.27
orbito-frontal gyri	38.42	4.84	42.76	4.04	41.94	5.64
inferior frontal gyrus	38.18	4.79	45.10	4.77	43.92	5.64
superior frontal gyrus	36.23	4.93	43.44	4.85	41.11	5.66
postcentral gyrus	35.39	4.60	43.90	4.53	42.04	5.96
superior parietal gyrus	38.55	4.63	46.63	4.32	46.60	6.42
lingual gyrus	42.33	4.46	47.20	4.42	47.67	6.59
cuneus	43.08	4.05	48.80	4.79	49.92	7.54

effects of volume, age and gender and compared these between our matched elderly control cohort and our patients. The parahippocampal gyrus revealed significant differences with a higher TSC in the patients' group compared to the controls' group. Other brain regions of the temporal lobe did not show group differences (Fig. S3A). In comparison, normalized TSC still showed influence of age and volume on several brain regions, but not of gender (Fig. S2). Furthermore, when regressing out the effect of volume, age and gender, normalized TSC revealed significant group differences in all temporal regions, except for the hippocampus (Fig. S3B).

3.5. Association between TSC increase and cognition in AD patients

In our voxel-wise regression model for MoCA ~ Sodium + Anatomical + Age + Gender, cognition represented by MoCA score is predicted by increased TSC in left temporal lobe, comprising hippocampus, parahippocampus as well as lateral structures of the temporal lobe (see also Fig. 5). Analysis on normalized TSC yielded similar results in our voxel-wise regression analysis.

3.6. High discriminative potential of normalized TSC between elderly controls and prodromal AD patients

When comparing normalized TSC regional maps in 8 regions from the Hammersmith atlas inside the temporal lobe (hippocampus, anterior medial and lateral temporal lobe, parahippocampus, superior temporal gyrus, inferior middle temporal gyrus, fusiform gyrus and posterior temporal lobe) between different patients' groups with CDR 0, CDR 0.5 and CDR 1 or 2, we state discriminative potential of normalized TSC between elderly control subjects and preclinical patients. After correction for multiple comparisons, most regions reveal a trend of significance for the comparison between elderly controls and preclinical patients with a CDR of 0, except for the posterior temporal lobe, revealing a significant effect ($zval = 2.72$; $p = 0.032$). In some regions, normalized TSC is further increasing along with disease progression represented by the CDR score (Fig. 6).

In a second step, we performed ROC-analyses to evaluate the discriminative potential of normalized TSC by comparing ROIs in the temporal lobe between elderly controls and patients at earliest stages of the disease (CDR 0 and CDR 0.5). For hippocampus, highest AUC was present for volume (0.88), normalized TSC yielded an AUC of 0.81. Interestingly, for other regions of the temporal lobe, normalized TSC surpasses volume and CT, such as for the anterior middle temporal lobe and seems to have a more widespread discriminative potential with AUC ranging between 0.76 and 0.82 in the temporal lobe (see Fig. 7).

3.7. Association of hippocampal TSC with CSF dementia marker

We did not find significant associations between normalized hippocampal TSC, and CSF markers (amyloid-1–42, amyloid-42/40-ratio, phospho-tau, tau). This was also the case for [Na^+] in CSF of the ventricles (both for quantitative as well as normalized TSC maps).

4. Discussion

In this work, we present data from a ^{23}Na-MRI study on a large and well-characterized sample of AD patients performed on a clinical 3T whole-body scanner. Next to quantitative TSC maps, we performed an analysis of normalized TSC maps, which was introduced to reduce the influence of the inter-individual-variability observed in the quantitative TSC maps in our group analysis. This variability could find its source in the fact that the physiological concentration of sodium in CSF follows a characteristic chronobiological rhythm which, in addition to the modest SNR available at 3T, may hinder a quantitative analysis of TSC changes

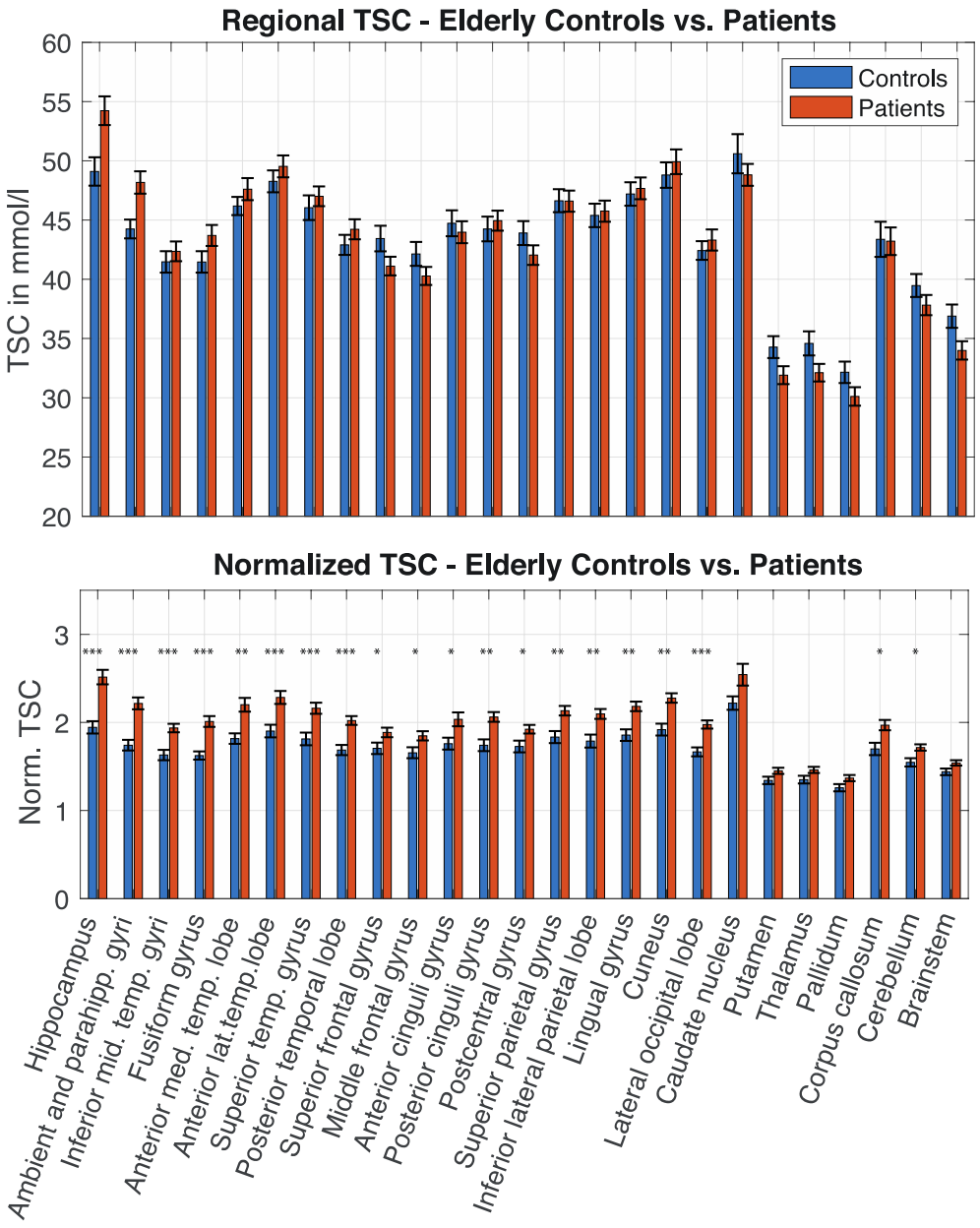

Fig. 3. TSC in mmol/l (above) and normalized TSC (below) in elderly controls subjects (n = 20) versus all AD patients (n = 52). *** $p < 0.001$; ** $p < 0.01$ * $p < 0.05$, otherwise not significant after correction for multiple comparison.

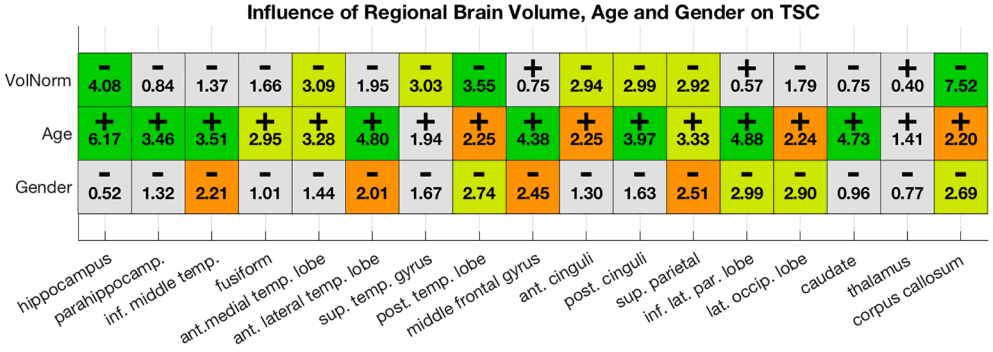

Fig. 4. *T*-values from multiple regression analysis on the influence of MoCA, Gender, Age and TIV-corrected volume (VolNorm) on the median TSC values across the 17 ROIs from the Hammersmith and VolBrain atlases. *T*-values (-,negative and +,positive) are presented, with colors indicating the significance level, orange when $p < 0.05$, yellow $p < 0.01$, green $p < 0.001$, grey when not significant. (For interpretation of the references to colour in this figure legend, the reader is referred to the web version of this article.)

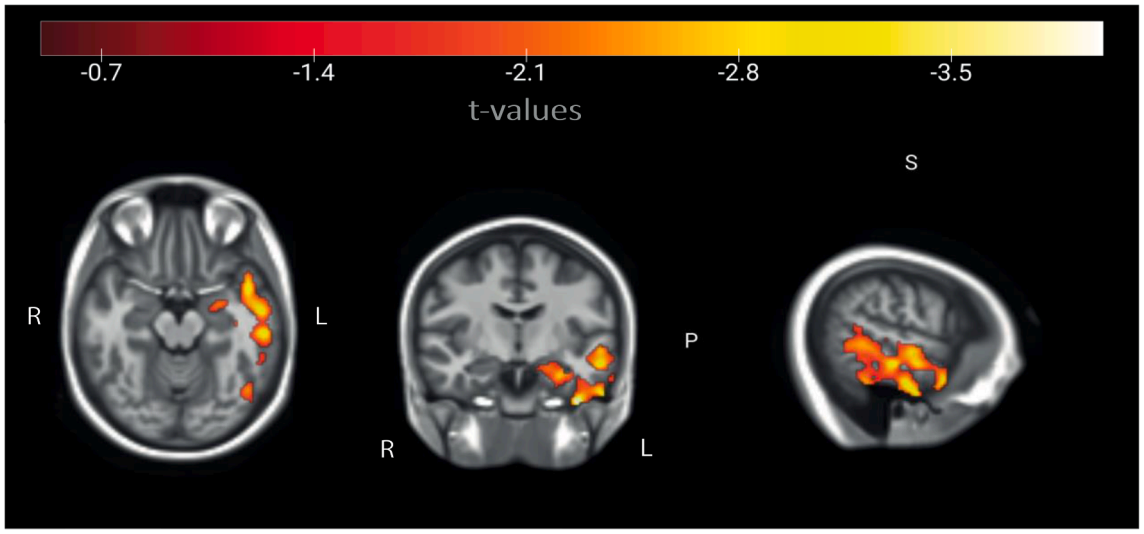

Fig. 5. Cluster results from the voxelwise regression analysis on the model MoCA ~ Sodium + Anatomical + Age + Gender. Negative *t*-values in the left temporal lobe point to a negative association in this region from TSC, with increased TSC implying a lower MoCA score. Results are presented RFT-corrected at $p < 0.05$.

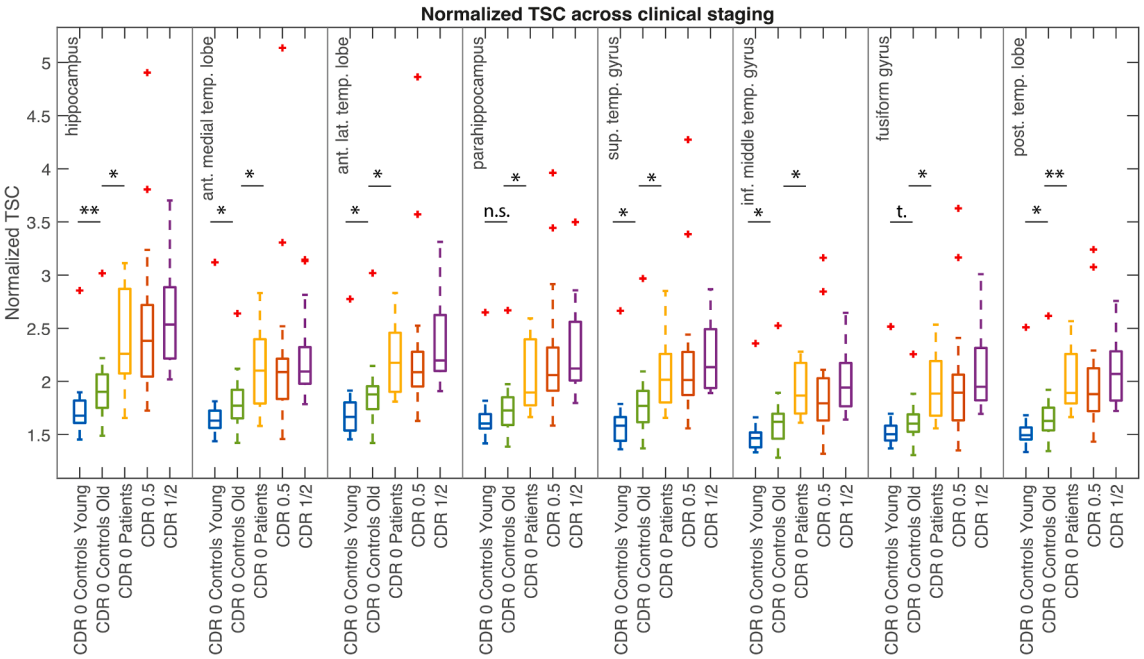

Fig. 6. Boxplots representing the median normalized TSC values across eight selected ROIs (hippocampus, anterior medial temporal lobe, anterior lateral temporal lobe, parahippocampus, superior temporal gyrus, inferior middle temporal gyri, fusiform gyrus, post. temporal lobe) for young controls (blue), elderly controls (green), patients with CDR = 0 (yellow), patients with CDR 0.5 (red), patients with CDR = 1 or 2 (purple). *** $p < 0.001$; ** $p < 0.01$ * $p < 0.05$, t. = trend, n.s. = not significant, no correction for multiple comparisons. Differences between elderly controls and patients with CDR = 0.5 and CDR = 1 or 2 are all significant, which is not separately illustrated here. (For interpretation of the references to colour in this figure legend, the reader is referred to the web version of this article.)

at the group level. A standard voxel-wise morphological study is presented as well.

Globally, we show that both quantitative as well as normalized TSC in AD patients are focally increased predominantly in regions of the temporal lobe with especially normalized TSC indicating a stage-dependent elevation of TSC levels: a pattern that we also observed under 7 T magnetic field condition (Haeger et al., 2021). Interestingly, when comparing TSC results with a younger control cohort to examine age-related effects, we found an increase of TSC with age independently of normalization.

We further specifically analyzed the influence of local brain volume, age, and gender in multiple regression models on local TSC in detail and confirm an influence mainly of the factors age and brain volume on local TSC in several brain regions, which seem to affect mainly quantitative TSC rather than the normalized TSC.

When linking TSC increase with cognition, we saw that increased TSC in the left temporal lobe is associated with lower MoCA score, i.e. worse cognition in our patients' group, independently of normalization.

For normalized TSC, which seems to be a more robust approach at 3T, we found that it displays an interesting ability to discriminate less affected patients with a low CDR of 0 and 0.5 from cognitively healthy elderly controls, making it a potentially powerful early imaging biomarker.

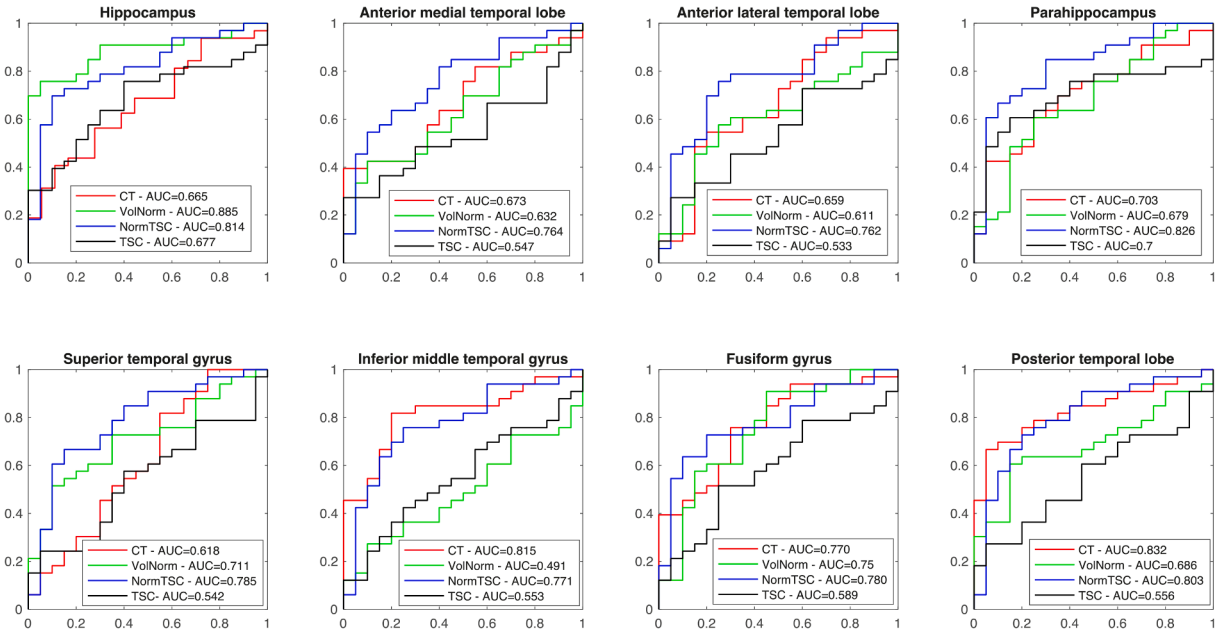

Fig. 7. ROC analysis with presented AUC for TSC (black), normalized TSC (NormTSC) (blue), Cortical Thickness (CT) (red), Normalized Volume (VolNorm) (green) in regions of the temporal lobe (Hippocampus, anterior medial temporal lobe, anterior lateral temporal lobe, parahippocampus, superior temporal grus, inferior middle temporal gyrus, fusiform gyrus, posterior temporal lobe) from the hammersmith/VolBrain atlases for effectiveness of discrimination between controls and cognitively less affected AD patients (CDR 0 or 0.5). (For interpretation of the references to colour in this figure legend, the reader is referred to the web version of this article.)

4.1. TSC increase in AD at 3T

This is the first ^{23}Na-MRI study of a large cohort of 52 well-classified AD patients at 3T. So far, there have been two previous ^{23}Na-MRI studies at 3T on few patients with AD which did not perform quantification but compared direct intensities from ^{23}Na-imaging (Mellon et al., 2009; Mohamed et al., 2021). One of the most important issues to be taken into consideration in ^{23}Na-MR imaging are partial-volume effects, especially in neurodegeneration which is prone to volume loss and therefore to strong influences coming from the high sodium concentration in CSF, an aspect which has rarely been tackled in ^{23}Na-MRI-studies before. In fact, to compensate for the low SNR of ^{23}Na-MRI performed at 3T, acquired images have relatively low resolutions (4 mm isotropic resolution) and are more prone to partial volume effects.

Furthermore, we present an additional normalization step derived from PET imaging analyses (de Souza et al., 2011; Goutal et al., 2020; Nugent et al., 2020) to reduce inter-individual variability in our sample and to therefore improve sensitivity of the technique at 3T. In such a way, we detected increases of normalized TSC on a whole brain level with a focus on temporal and occipital lobes. At the ROI-level, we found normalized TSC increases in most brain regions typically affected by AD pathology except for subcortical regions. It is therefore advisable to perform a normalization of TSC, at least when there is a risk of high interindividual-variability, to take into account lower SNR and possible circadian rhythm effects which might be due to different acquisition time points across the day (Harrington et al., 2010). Normalization to an intracerebral brain region therefore resolves these effects and, as we can show, is clinically more powerful in discriminating between control subjects and only mildly affected patients with CDR of 0/0.5. Similar to PET-imaging, we also performed normalization to a brain region less prone to AD-pathology, i.e. the brainstem. We did not choose e.g. the ventricles, since CSF sodium values have also recently been detected to change in AD-pathology and those at risk for it (Babić Leko et al., 2021; Souza et al., 2020).

4.2. Influence of local volume, age and gender on TSC

In our multiple regression analysis, local brain volume, age, and gender were significant predictors for TSC for most of the selected ROIs. Volume loss is a direct consequence of neurodegeneration. It is therefore not surprising that brain volume is associated with increased TSC as a parameter for possible disturbed cell homeostasis in this region. Thulborn et al. (2016) closely analyzed this aspect at 9.4 T and showed, thanks to the high-resolution images that they obtained, that no change in TSC depending on age is found in brain tissues. However, the same study also showed a progressive increase of CSF in the brain. Therefore, it cannot be ruled out that the TSC increase that we observed was driven by the low resolution of sodium images in combination with increased volume loss. Particularly at 3T with a resolution of 4 mm, partial volume effects due to an increase of extracellular space can rule in when regarding the interaction of atrophy and TSC increase. The effect of gender might also be related to different brain volumes (Ritchie et al., 2018; Ruigrok et al., 2014) but might also go beyond with a relation to metabolic differences between the female and male brain (Feng et al., 2022; Malpetti et al., 2017). The effect of gender on cell volume fraction (CVF) was also recently discussed by Thulborn, 2022. Nevertheless, when regressing out the factor brain volume, as well as age and gender, we still observed group differences for normalized TSC showing that effects go beyond volume-influences.

4.3. TSC as possible negative predictor for cognition

We performed a voxel-wise regression analysis to examine the association of TSC with the MoCA score, and included the factors brain volume, age and gender in our regression model. We found that increased TSC in the left temporal lobe is associated with cognitive decline in our AD cohort, represented by a lower MoCA score. Previous literature has already pointed to an asymmetrical distribution of AD pathology (Raji et al., 2008; Weise et al., 2018) and since the MoCA is a language-focused test, it might explain the left-dominant lateralization. This is also confirmed by the fact, that except for one patient reporting to be ambidextrous and two patients reporting to be left-handed, all

participating patients from our sample were right-handed and only one elderly control subject was ambidextrous.

4.4. Normalization of TSC leading to high discriminative potential

Finally, we moved back from quantification and set our focus on normalized TSC for reduction of inter-subject variability. Furthermore, sodium follows a circadian rhythms (Harrington et al., 2010). With the normalization methods, we could reduce these possible inter-individual fluctuations, which are likely at different acquisitions times. Interestingly, we observed an improved separation between the different stages (Fig. 6). This is also reflected by our ROC-analysis (Fig. 7). We found that for the hippocampus, the AUC for volume was still higher than for TSC. However, for other regions of the temporal lobe, there was a higher AUC for TSC compared to volume and cortical thickness. One can assume that hippocampal volume is a powerful driver of stage-prediction, as we have seen from previous studies (Coupé et al., 2019; Mungas et al., 2005). TSC, in contrast, seems to be a more general predictor of AD progression since it reveals relatively high AUCs compared to volume and cortical thickness also in other brain regions of the temporal lobe. This more widespread discriminative power of TSC outside the hippocampus could be due to the fact that disturbances in tissue homeostasis might precede the onset of significant atrophy. An increase in TSC has already been confirmed in *post mortem* examinations of brain tissue of AD patients (Graham et al., 2015; Vitvitsky et al., 2012) and in AD patients at risk (Babić Leko et al., 2021; Souza et al., 2020).

There are several possible explanations for sodium increase in AD. One possibility is that there is already a failure in mitochondrial energy synthesis, leading to a lack of adenosine-triphosphate (ATP) finally resulting in malfunctions of the Na^+/K^+-ATPase which is essential for maintaining the cellular resting potential. This would be in concordance with the observations of TSC increases in other diseases with known mitochondrial deficits such as e.g. Huntington' s disease (Damiano et al., 2010; Jodeiri Farshbaf and Ghaedi, 2017; Reetz et al., 2012) and could also explain why there would be a strong association with age and brain volume, since mitochondrial function is declining with aging possibly due to accumulated stress from reactive oxygen species (Haas, 2019; Sun et al., 2016). Another possible influence remains the increasing volume loss during aging. Therefore, we calculated the residuals without influence of age, gender and volume. Interestingly, TSC increase in the hippocampus seems to be especially driven by these factors, maybe also due to the general high-volume loss of the hippocampus in AD. We did not find any correlation between TSC in the hippocampus or the ventricles and the CSF biomarkers for dementia, though. However, this might also be due to the fact that CSF markers were assessed during the diagnostic process and not necessarily at the same time point as the MRI assessment.

One of the contributions of this study is the possibility of using normalized TSC as a robust biomarker to discriminate very mildly affected AD patients from elderly controls. Indeed, we observed a promising statistical trend of significance (after correction for multiple comparisons) in the normalized TSC values from temporal ROIs between elderly controls and the subgroup of AD patients with CDR 0 despite its small size ($n = 8$).

One of the main challenges of ^{23}Na-MRI are partial volume effects. These are especially manifest in studies of neurodegenerative diseases for which there are large CSF volume increases and concomitant brain volume loss. So far, most studies on ^{23}Na-MRI have not considered partial volume effects. Next to a partial volume correction, we also performed a thorough coregistration and masked for CSF to exclude possible intensity influences coming from CSF. Still, there might be a remaining impact, which cannot be ruled out, especially under lower magnetic field conditions compared to ultra-high field (Haeger et al., 2021). The etiology of TSC increase in AD therefore needs to be further scrutinized, e.g. by brain tissue multi-compartment modelling of its sodium content.

5. Conclusions

We here present results from a ^{23}Na- multimodal MR imaging study at 3T in a large sample of 52 AD patients, and 34 cognitively healthy subjects. We show that under 3T magnetic field strength, normalization of TSC may allow for a better discrimination between elderly control subjects and mildly affected patients as compared to quantitative TSC measurements. In several regions of the temporal lobe, normalized TSC has an even higher discriminative power compared to classical tools of volume and cortical thickness assessment. Interestingly, TSC is strongly age- and volume-driven and is linked to the cognitive decline of patients. TSC might therefore serve as a potential marker of cellular energy depletion and disturbed homeostasis, associated with the different states of cognitive decline. TSC could therefore be useful in clinical trials for the evaluation of intervention effects, with a potential metabolic focus. The etiology of TSC increase, its relation to the hypometabolism and its role in the pathophysiology of AD need to be further examined in further studies.

6. Data availability

The data that support the findings of this study are available from the corresponding author upon reasonable request.

Funding

KR and SR were partly funded by the German Federal Ministry of Education and Research (BMBF 01GQ1402 to KR). AH received funding through the START-Program (121/18), RWTH-Startup grant (StUpPD_329- 18) and a research fellowship of the Faculty of Medicine, RWTH Aachen University Hospital.

CRediT authorship contribution statement

Alexa Haeger: Conceptualization, Data curation, Formal analysis, Investigation, Methodology, Project administration, Software, Validation, Visualization, Funding acquisition, Writing – original draft. **Fawzi Boumezbeur:** Writing – review & editing. **Michel Bottlaender:** Writing – review & editing. **Cécile Rabrait-Lerman:** Writing – review & editing. **Julien Lagarde:** Writing – review & editing. **Shahram Mirzazade:** Data curation, Writing – review & editing. **Janna Krahe:** Writing – review & editing. **Christian Hohenfeld:** Data curation, Validation, Writing – review & editing. **Marie Sarazin:** Writing – review & editing. **Jörg B. Schulz:** Resources, Writing – review & editing. **Sandro Romanzetti:** Conceptualization, Data curation, Formal analysis, Methodology, Software, Validation, Writing – review & editing. **Kathrin Reetz:** Conceptualization, Funding acquisition, Methodology, Project administration, Resources, Supervision, Validation, Writing – review & editing.

Declaration of Competing Interest

The authors declare that they have no known competing financial interests or personal relationships that could have appeared to influence the work reported in this paper.

Data availability

Data will be made available on request.

Appendix A. Supplementary data

Supplementary data to this article can be found online at https://doi.org/10.1016/j.nicl.2022.103274.

References

Avants, B.B., Tustison, N.J., Song, G., Cook, P.A., Klein, A., Gee, J.C., 2011. A reproducible evaluation of ANTs similarity metric performance in brain image registration. Neuroimage 54, 2033–2044. https://doi.org/10.1016/j.neuroimage.2010.09.025.

Babić Leko, M., Jurasović, J., Nikolac Perković, M., Španić, E., Sekovanić, A., Orct, T., Lukinović Škudar, V., Bačić Baronica, K., Kiđemet-Piskač, S., Vogrinc, Ž., Pivac, N., Borovečki, F., Hof, P.R., Šimić, G., 2021. The Association of Essential Metals with APOE Genotype in Alzheimer's Disease. J. Alzheimer's Dis. Preprint 82 (2), 661–672.

Bauer, M., C.,, 2013. Differentiating between Normal Aging, Mild Cognitive Impairment, and Alzheimer's disease with FDG-PET: Effects of Normalization Region and Partial Volume Correction Method. J. Alzheimer's Dis. Parkinsonism 03, 1–9. https://doi.org/10.4172/2161-0460.1000113.

Beck, A.T., Steer, R.A., Brown, G.K., 1996. Manual for the beck depression inventory-II. The Psychological Corporation. San Antonio, TX 1996.

Boada, F.E., LaVerde, G., Jungreis, C., Nemoto, E., Tanase, C., Hancu, I., 2005. Loss of Cell Ion Homeostasis and Cell Viability in the Brain: What Sodium MRI Can Tell Us. Curr. Top. Dev. Biol. https://doi.org/10.1016/S0070-2153(05)70004-1.

Costa, A., Boumezbeur, F., Vignaud, A., et al., 2019. Tissue sodium concentration and sodium T 1 mapping of the human brain at 3 T using a Variable Flip Angle method. Magn. Reson. Imaging 58, 116–124. https://doi.org/10.1016/j.mri.2019.01.015.

Coupé, P., Manjón, J.V., Lanuza, E., Catheline, G., 2019. Lifespan Changes of the Human Brain In Alzheimer's Disease. Sci. Rep. 9, 1–12. https://doi.org/10.1038/s41598-019-39809-8.

Cummings, J.L., Doody, R., Clark, C., 2007. Disease-modifying therapies for Alzheimer disease: Challenges to early intervention. Neurology 69 (16), 1622–1634.

Damiano, M., Galvan, L., Déglon, N., Brouillet, E., 2010. Mitochondria in Huntington's disease. Biochim. Biophys. Acta (BBA) - Mol. Basis Dis. 1802, 52–61. https://doi.org/10.1016/j.bbadis.2009.07.012.

de Souza, L.C., Corlier, F., Habert, M.-O., Uspenskaya, O., Maroy, R., Lamari, F., Chupin, M., Lehéricy, S., Colliot, O., Hahn-Barma, V., Samri, D., Dubois, B., Bottlaender, M., Sarazin, M., 2011. Similar amyloid-β burden in posterior cortical atrophy and Alzheimer's disease. Brain 134, 2036–2043. https://doi.org/10.1093/brain/awr130.

Eklund, A., Dufort, P., Villani, M., LaConte, S., 2014. BROCCOLI: Software for fast fMRI analysis on many-core CPUs and GPUs. Front. Neuroinf. 8 https://doi.org/10.3389/fninf.2014.00024.

Feng, B., Cao, J., Yu, Y., Yang, H., Jiang, Y., Liu, Y., Wang, R., Zhao, Q., 2022. Gender-Related Differences in Regional Cerebral Glucose Metabolism in Normal Aging Brain. Front. Aging Neurosci. 14, 55. https://doi.org/10.3389/fnagi.2022.809767.

Folstein, M.F., Folstein, S.E., McHugh, P.R., 1975. Mini-Mental State; a practical method for grading the cognitive state of patients for the clinician. J. gsychiaf. Res 12 (3), 189–198.

Fox, N.C., Cousens, S., Scahill, R., Harvey, R.J., Rossor, M.N., 2000. Using serial registered brain magnetic resonance imaging to measure disease progression in Alzheimer disease: Power calculations and estimates of sample size to detect treatment effects. Arch. Neurol. 57, 339–344. https://doi.org/10.1001/archneur.57.3.339.

Frisoni, G.B., Fox, N.C., Jack, C.R., Scheltens, P., Thompson, P.M., 2010. The clinical use of structural MRI in Alzheimer disease. Nat. Rev. Neurol. 6 (2), 67–77.

Goutal, S., Tournier, N., Guillermier, M., Van Camp, N., Barret, O., Gaudin, M., Bottlaender, M., Hantraye, P., Lavisse, S., Baucknehť, M., 2020. Comparative test-retest variability of outcome parameters derived from brain [18F]FDG PET studies in non-human primates. PLoS One 15 (10), e0240228.

Graham, S.F., Nasarauddin, M.B., Carey, M., McGuinness, B., Holscher, C., Kehoe, P.G., Love, S., Passmore, A.P., Elliott, C.T., Meharg, A., Green, B.D., 2015. Quantitative measurement of [Na+] and [K+] in postmortem human brain tissue indicates disturbances in subjects with Alzheimer's disease and dementia with Lewy bodies. Journal of Alzheimer's Disease 44, 851–857. https://doi.org/10.3233/JAD-141869.

Haas, R.H., 2019. Mitochondrial Dysfunction in Aging and Diseases of Aging. Biology 8, 48. https://doi.org/10.3390/biology8020048.

Haeger, A., Costa, A.S., Romanzetti, S., Kilders, A., Trautwein, C., Haberl, L., Beulertz, M., Hildebrand, F., Schulz, J.B., Reetz, K., 2020. Effect of a multicomponent exercise intervention on brain metabolism: A randomized controlled trial on Alzheimer's pathology (Dementia-MOVE). Alzheimer's & Dementia: Transl. Res. Clin. Intervent. 6 https://doi.org/10.1002/trc2.12032.

Haeger, A., Bottlaender, M., Lagarde, J., Porciuncula Baptista, R., Rabrait-Lerman, C., Luecken, V., Schulz, J.B., Vignaud, A., Sarazin, M., Reetz, K., Romanzetti, S., Boumezbeur, F., 2021. What can 7T sodium MRI tell us about cellular energy depletion and neurotransmission in Alzheimer's disease? Alzheimer's & Dementia 17, 1843–1854. https://doi.org/10.1002/alz.12501.

Hammers, A., Allom, R., Koepp, M.J., Free, S.L., Myers, R., Lemieux, L., Mitchell, T.N., Brooks, D.J., Duncan, J.S., 2003. Three-dimensional maximum probability atlas of the human brain, with particular reference to the temporal lobe. Hum. Brain Mapp. 19, 224–247. https://doi.org/10.1002/hbm.10123.

Harrington, M.G., Salomon, R.M., Pogoda, J.M., Oborina, E., Okey, N., Johnson, B., Schmidt, D., Fonteh, A.N., Dalleska, N.F., 2010. Cerebrospinal fluid sodium rhythms. Cerebrospinal Fluid Res. 7, 3. https://doi.org/10.1186/1743-8454-7-3.

Holtzman, D.M., Morris, J.C., Goate, A.M., 2011. Alzheimer's disease: The challenge of the second century. Sci. Transl. Med. 3 (77) https://doi.org/10.1126/scitranslmed.3002369.

Huang, L.-K., Chao, S.-P., Hu, C.-J., 2020. Clinical trials of new drugs for Alzheimer disease. J. Biomed. Sci. 27 (1) https://doi.org/10.1186/s12929-019-0609-7.

Inglese, M., Madelin, G., Oesingmann, N., Babb, J.S., Wu, W., Stoeckel, B., Herbert, J., Johnson, G., 2010. Brain tissue sodium concentration in multiple sclerosis: a sodium imaging study at 3 tesla. Brain J. Neurol. 133, 847–857. https://doi.org/10.1093/brain/awp334.

Ishii, K., 2002. Clinical application of positron emission tomography for diagnosis of dementia. Ann. Nucl. Med. 16, 515–525. https://doi.org/10.1007/BF02988628.

Jack, C.R., Bennett, D.A., Blennow, K., Carrillo, M.C., Dunn, B., Haeberlein, S.B., Holtzman, D.M., Jagust, W., Jessen, F., Karlawish, J., Liu, E., Molinuevo, J.L., Montine, T., Phelps, C., Rankin, K.P., Rowe, C.C., Scheltens, P., Siemers, E., Snyder, H.M., Sperling, R., Elliott, C., Masliah, E., Ryan, L., Silverberg, N., 2018. NIA-AA Research Framework: Toward a biological definition of Alzheimer's disease. Alzheimer's & Dementia 14 (4), 535–562.

Jenkinson, M., Beckmann, C.F., Behrens, T.E.J., Woolrich, M.W., Smith, S.M., 2012. FSL. FSL. NeuroImage 62 (2), 782–790.

Jodeiri Farshbaf, M., Ghaedi, K., 2017. Huntington's Disease and Mitochondria. Neurotox. Res. 32, 518–529. https://doi.org/10.1007/s12640-017-9766-1.

Madelin, G., Regatte, R.R., 2013. Biomedical applications of sodium MRI in vivo. J. Magn. Reson. Imaging 38, 511–529. https://doi.org/10.1002/jmri.24168.

Malpetti, M., Ballarini, T., Presotto, L., Garibotto, V., Tettamanti, M., Perani, D., 2017. Gender differences in healthy aging and Alzheimer's Dementia: A 18 F-FDG-PET study of brain and cognitive reserve. Hum. Brain Mapp. 38 (8), 4212–4227.

Manjón, J.V., Coupé, P., 2016. volBrain: An Online MRI Brain Volumetry System. Front. Neuroinf. 10, 30. https://doi.org/10.3389/fninf.2016.00030.

Mathotaarachchi, S., Wang, S., Shin, M., Pascoal, T.A., Benedet, A.L., Kang, M.S., Beaudry, T., Fonov, V.S., Gauthier, S., Labbe, A., Rosa-Neto, P., 2016. VoxelStats: A MATLAB Package for Multi-Modal Voxel-Wise Brain Image Analysis. Front. Neuroinf. 10, 20. https://doi.org/10.3389/fninf.2016.00020.

McDonald, C.R., McEvoy, L.K., Gharapetian, L., Fennema-Notestine, C., Hagler, D.J., Holland, D., Koyama, A., Brewer, J.B., Dale, A.M., 2009. Regional rates of neocortical atrophy from normal aging to early Alzheimer disease. Neurology 73 (6), 457–465.

Mellon, E.A., Pilkinton, D.T., Clark, C.M., Elliott, M.A., Witschey, W.R., Borthakur, A., Reddy, R., 2009. Sodium MR Imaging Detection of Mild Alzheimer Disease: Preliminary Study. Am. J. Neuroradiol. 30 (5), 978–984.

Mohamed, S.A., Herrmann, K., Adlung, A., Paschke, N., Hausner, L., Frölich, L., Schad, L., Groden, C., Kerl, H.U., 2021. Evaluation of Sodium (23 Na) MR-imaging as a Biomarker and Predictor for Neurodegenerative Changes in Patients With Alzheimer's Disease. In Vivo 35, 429–435. https://doi.org/10.21873/invivo.12275.

Morris, J.C., 1993. The clinical dementia rating (cdr): Current version and scoring rules. Neurology 43, 2412–2414. https://doi.org/10.1212/wnl.43.11.2412-a.

Mungas, D., Harvey, D., Reed, B.R., Jagust, W.J., DeCarli, C., Beckett, L., Mack, W.J., Kramer, J.H., Weiner, M.W., Schuff, N., Chui, H.C., 2005. Longitudinal volumetric MRI change and rate of cognitive decline. Neurology 65, 565–571. https://doi.org/10.1212/01.wnl.0000172913.88973.0d.

Nichols, E., Szoeke, C.E.I., Vollset, S.E., Abbasi, N., Abd-Allah, F., Abdela, J., Aichour, M. T.E., Akinyemi, R.O., Alahdab, F., Asgedom, S.W., Awasthi, A., Barker-Collo, S.L., Baune, B.T., Béjot, Y., Belachew, A.B., Bennett, D.A., Biadgo, B., Bijani, A., Bin Sayeed, M.S., Brayne, C., Carpenter, D.O., Carvalho, F., Catalá-López, F., Cerin, E., Choi, J.-Y., Dang, A.K., Degefa, M.G., Djalalinia, S., Dubey, M., Duken, E.E., Edvardsson, D., Endres, M., Eskandarieh, S., Faro, A., Farzadfar, F., Fereshtehnejad, S.-M., Fernandes, E., Filip, I., Fischer, F., Gebre, A.K., Geremew, D., Ghasemi-Kasman, M., Gnedovskaya, E.V., Gupta, R., Hachinski, V., Hagos, T.B., Hamidi, S., Hankey, G.J., Haro, J.M., Hay, S.I., Irvani, S.S.N., Jha, R.P., Jonas, J.B., Kalani, R., Karch, A., Kasaeian, A., Khader, Y.S., Khalil, I.A., Khan, E.A., Khanna, T., Khoja, T.A.M., Khubchandani, J., Kisa, A., Kissimova-Skarbek, K., Kivimäki, M., Koyanagi, A.i., Krohn, K.J., Logroscino, G., Lorkowski, S., Majdan, M., Malekzadeh, R., März, W., Massano, J., Mengistu, G., Meretoja, A., Mohammadi, M., Mohammadi-Khanaposhtani, M., Mokdad, A.H., Mondello, S., Moradi, G., Nagel, G., Naghavi, M., Naik, G., Nguyen, L.H., Nguyen, T.H., Nirayo, Y.L., Nixon, M.R., Ofori-Asenso, R., Ogbo, F.A., Olagunju, A.T., Owolabi, M.O., Panda-Jonas, S., Passos, V.M. d.A., Pereira, D.M., Pinilla-Monsalve, G.D., Piradov, M.A., Pond, C.D., Poustchi, H., Qorbani, M., Radfar, A., Reiner, R.C., Robinson, S.R., Roshandel, G., Rostami, A., Russ, T.C., Sachdev, P.S., Safari, H., Safiri, S., Sahathevan, R., Salimi, Y., Satpathy, M., Sawhney, M., Saylan, M., Sepanlou, S.G., Shafieesabet, A., Shaikh, M. A., Sahraian, M.A., Shigematsu, M., Shiri, R., Shiue, I., Silva, J.P., Smith, M., Sobhani, S., Stein, D.J., Tabarés-Seisdedos, R., Tovani-Palone, M.R., Tran, B.X., Tran, T.T., Tsegay, A.T., Ullah, I., Venketasubramanian, N., Vlassov, V., Wang, Y.-P., Weiss, J., Westerman, R., Wijeratne, T., Wyper, G.M.A., Yano, Y., Yimer, E.M., Yonemoto, N., Yousefifard, M., Zaidi, Z., Zare, Z., Vos, T., Feigin, V.L., Murray, C.J. L., 2019. Global, regional, and national burden of Alzheimer's disease and other dementias, 1990–2016: a systematic analysis for the Global Burden of Disease Study 2016. Lancet Neurol. 18 (1), 88–106.

Nielles-Vallespin, S., Weber, M.-A., Bock, M., Bongers, A., Speier, P., Combs, S.E., Wöhrle, J., Lehmann-Horn, F., Essig, M., Schad, L.R., 2007. 3D radial projection technique with ultrashort echo times for sodium MRI: Clinical applications in human brain and skeletal muscle. Magn. Reson. Med. 57, 74–81. https://doi.org/10.1002/mrm.21104.

Nordberg, A., Rinne, J.O., Kadir, A., Långström, B., 2010. The use of PET in Alzheimer disease. Nat. Rev. Neurol. 6, 78–87. https://doi.org/10.1038/nrneurol.2009.217.

Nugent, S., Croteau, E., Potvin, O., Castellano, C.A., Dieumegarde, L., Cunnane, S.C., Duchesne, S., 2020. Selection of the optimal intensity normalization region for FDG-PET studies of normal aging and Alzheimer's disease. Sci. Rep. 10 https://doi.org/10.1038/S41598-020-65957-3.

Pipe, J.G., Zwart, N.R., Aboussouan, E.A., Robison, R.K., Devaraj, A., Johnson, K.O., 2011. A new design and rationale for 3D orthogonally oversampled k-space

trajectories. Magn. Reson. Med. 66, 1303–1311. https://doi.org/10.1002/mrm.22918.
Raji, C.A., Becker, J.T., Tsopelas, N.D., Price, J.C., Mathis, C.A., Saxton, J.A., Lopresti, B. J., Hoge, J.A., Ziolko, S.K., DeKosky, S.T., Klunk, W.E., 2008. Characterizing regional correlation, laterality and symmetry of amyloid deposition in mild cognitive impairment and Alzheimer's disease with Pittsburgh Compound B. J. Neurosci. Methods 172, 277–282. https://doi.org/10.1016/J.JNEUMETH.2008.05.005.
Reetz, K., Romanzetti, S., Dogan, I., Saß, C., Werner, C.J., Schiefer, J., Schulz, J.B., Shah, N.J., 2012. Increased brain tissue sodium concentration in Huntington's Disease — A sodium imaging study at 4T. Neuroimage 63, 517–524. https://doi.org/10.1016/j.neuroimage.2012.07.009.
Regnery, S., Behl, N.G.R., Platt, T., Weinfurtner, N., Windisch, P., Deike-Hofmann, K., Sahm, F., Bendszus, M., Debus, J., Ladd, M.E., Schlemmer, H.P., Rieken, S., Adeberg, S., Paech, D., 2020. Ultra-high-field sodium MRI as biomarker for tumor extent, grade and IDH mutation status in glioma patients. NeuroImage: Clinical 28, 102427. https://doi.org/10.1016/j.nicl.2020.102427.
Reiber, H., 2005. Liquordiagnostik: Labor und Diagnose. TH Books, Frankfurt.
S.J. Ritchie S.R. Cox X. Shen M.V. Lombardo L.M. Reus C. Alloza M.A. Harris H.L. Alderson S. Hunter E. Neilson D.C.M. Liewald B. Auyeung H.C. Whalley S.M. Lawrie C.R. Gale M.E. Bastin A.M. McIntosh I.J. Deary Sex Differences in the Adult Human Brain: Evidence from 5216 UK Biobank Participants 28 8 2018 2018 2959 2975.
Romanzetti, S., Mirkes, C.C., Fiege, D.P., Celik, A., Felder, J., Shah, N.J., 2014. Mapping tissue sodium concentration in the human brain: A comparison of MR sequences at 9.4Tesla. Neuroimage 96, 44–53. https://doi.org/10.1016/j.neuroimage.2014.03.079.
Ruigrok, A.N.V., Salimi-Khorshidi, G., Lai, M.C., Baron-Cohen, S., Lombardo, M.V., Tait, R.J., Suckling, J., 2014. A meta-analysis of sex differences in human brain structure. Neurosci. Biobehav. Rev. 39, 34–50. https://doi.org/10.1016/J.NEUBIOREV.2013.12.004.
Scheltens, P., De Strooper, B., Kivipelto, M., Holstege, H., Chételat, G., Teunissen, C.E., Cummings, J., van der Flier, W.M., 2021. Alzheimer's disease. Lancet 397, 1577–1590. https://doi.org/10.1016/S0140-6736(20)32205-4.
Shah, N.J., Worthoff, W.A., Langen, K.-J., 2016. Imaging of sodium in the brain: a brief review. NMR Biomed. 29, 162–174. https://doi.org/10.1002/nbm.3389.
Souza, L.A.C., Trebak, F., Kumar, V., Satou, R., Kehoe, P.G., Yang, W., Wharton, W., Earley, Y.F., 2020. Elevated cerebrospinal fluid sodium in hypertensive human subjects with a family history of Alzheimer's disease. Physiol. Genomics 52, 133–142. https://doi.org/10.1152/physiolgenomics.00093.2019.
Sun, N., Youle, R.J., Finkel, T., 2016. The Mitochondrial Basis of Aging. Mol. Cell 61, 654–666. https://doi.org/10.1016/j.molcel.2016.01.028.
Thomas, B.A., Cuplov, V., Bousse, A., Mendes, A., Thielemans, K., Hutton, B.F., Erlandsson, K., 2016. PETPVC: A toolbox for performing partial volume correction techniques in positron emission tomography. Phys. Med. Biol. 61, 7975–7993. https://doi.org/10.1088/0031-9155/61/22/7975.
Thulborn, K.R., 2018. Quantitative sodium MR imaging: A review of its evolving role in medicine. Neuroimage 168, 250–268. https://doi.org/10.1016/j.neuroimage.2016.11.056.
Thulborn, K.R., 2022. Gender differences in cell volume fraction (CVF): a structural parameter reflecting the energy efficiency of maintaining the resting membrane potential. NMR Biomed. 35 (7).
Thulborn, K.R., Davis, D., Adams, H., Gindin, T., Zhou, J., 1999. Quantitative Tissue Sodium Concentration Mapping of the Growth of Focal Cerebral Tumors With Sodium Magnetic Resonance Imaging. Magn. Reson. Med. https://doi.org/10.1002/(SICI)1522-2594(199902)41:2.
Thulborn, K., Lui, E., Guntin, J., Jamil, S., Sun, Z., Claiborne, T.C., Atkinson, I.C., 2016. Quantitative sodium MRI of the human brain at 9.4 T provides assessment of tissue sodium concentration and cell volume fraction during normal aging. NMR Biomed. 29, 137–143. https://doi.org/10.1002/nbm.3312.
Tustison, N.J., Cook, P.A., Klein, A., Song, G., Das, S.R., Duda, J.T., Kandel, B.M., van Strien, N., Stone, J.R., Gee, J.C., Avants, B.B., 2014. Large-scale evaluation of ANTs and FreeSurfer cortical thickness measurements. Neuroimage 99, 166–179. https://doi.org/10.1016/j.neuroimage.2014.05.044.
Vitvitsky, V.M., Garg, S.K., Keep, R.F., Albin, R.L., Banerjee, R., 2012. Na + and K + ion imbalances in Alzheimer's disease. Biochim. Biophys. Acta Mol. basis Dis. 1822, 1671–1681. https://doi.org/10.1016/j.bbadis.2012.07.004.
Weise, C.M., Chen, K., Chen, Y., Kuang, X., Savage, C.R., Reiman, E.M., 2018. Left lateralized cerebral glucose metabolism declines in amyloid-β positive persons with mild cognitive impairment. NeuroImage: Clinical 20, 286–296. https://doi.org/10.1016/J.NICL.2018.07.016.
Zettl, U., Lehmitz, R., Mix, E., 2005. Klinische Liquordiagnostik. De Gruyter, Berlin.